Present-day surface deformation and tectonic insights of the extensional Ilan Plain, NE Taiwan

Chu-Chun Kang [a], Chung-Pai Chang [a,b,e,*], Lionel Siame [c,d,a,e], Jian-Cheng Lee [d,e]

[a] Institute of Geophysics, National Central University, Chungli 320, Taiwan
[b] Geological Remote Sensing Laboratory, Center for Space and Remote Sensing Research, National Central University, Chungli 320, Taiwan
[c] Aix-Marseille Université, CNRS-IRD-Collège de France, UM 34 CEREGE, Technopôle de l'Arbois, BP80, 13545 Aix-en-Provence, France
[d] Institute of Earth Sciences, Academia Sinica, P.O. Box 1-55, 128, Sec. 2, Academia Road, Nangang, Taipei 11529, Taiwan
[e] LIA (Associated International Laboratory), ADEPT (Active Deformation and Environment Programme for Taiwan), Centre National de la Recherche Scientifique/Institut National des Sciences de l'Univers (France), National Science Council, Taiwan

ARTICLE INFO

ABSTRACT

Taiwan's mountain belt is an ideal location to address major questions regarding mechanisms of litho-spheric deformation in convergent settings, mountain building processes from oceanic subduction to continental subduction, and post orogenic extension. In the northeast of this belt, the Ilan Plain is a tri-angular, deltaic plain characterized by a flat topography close to the sea level, and surrounded by the high mountains of the Hsuehshan Range to the northwest, and the Central Range to the southeast. Its eastern coast faces the western tip of the Okinawa Trough, the back-arc basin of the Ryukyu subduction zone. In this study, we analyzed the present-day surface deformation of the Ilan Plain, aiming at deciphering its relationships with basement faults and the regional geodynamic setting. Our approach is mainly based on surface vertical displacements revealed by Persistent Scatterer Interferometry Synthetic Aperture Radar (PSI), which indicate that there is an area of active subsidence (~18 mm/yr) located in the southern part of the plain in probable connection with active basement faults and in agreement with previous geodetic measurements and existing geophysical data. Our PSI results also suggest that the subsidence occurring in the Ilan Plain has moved from north to south during Quaternary in relation with extrusion of the belt due to the westward propagation of the Okinawa Trough through the Taiwan Mountains.

© 2015 Elsevier Ltd. All rights reserved.
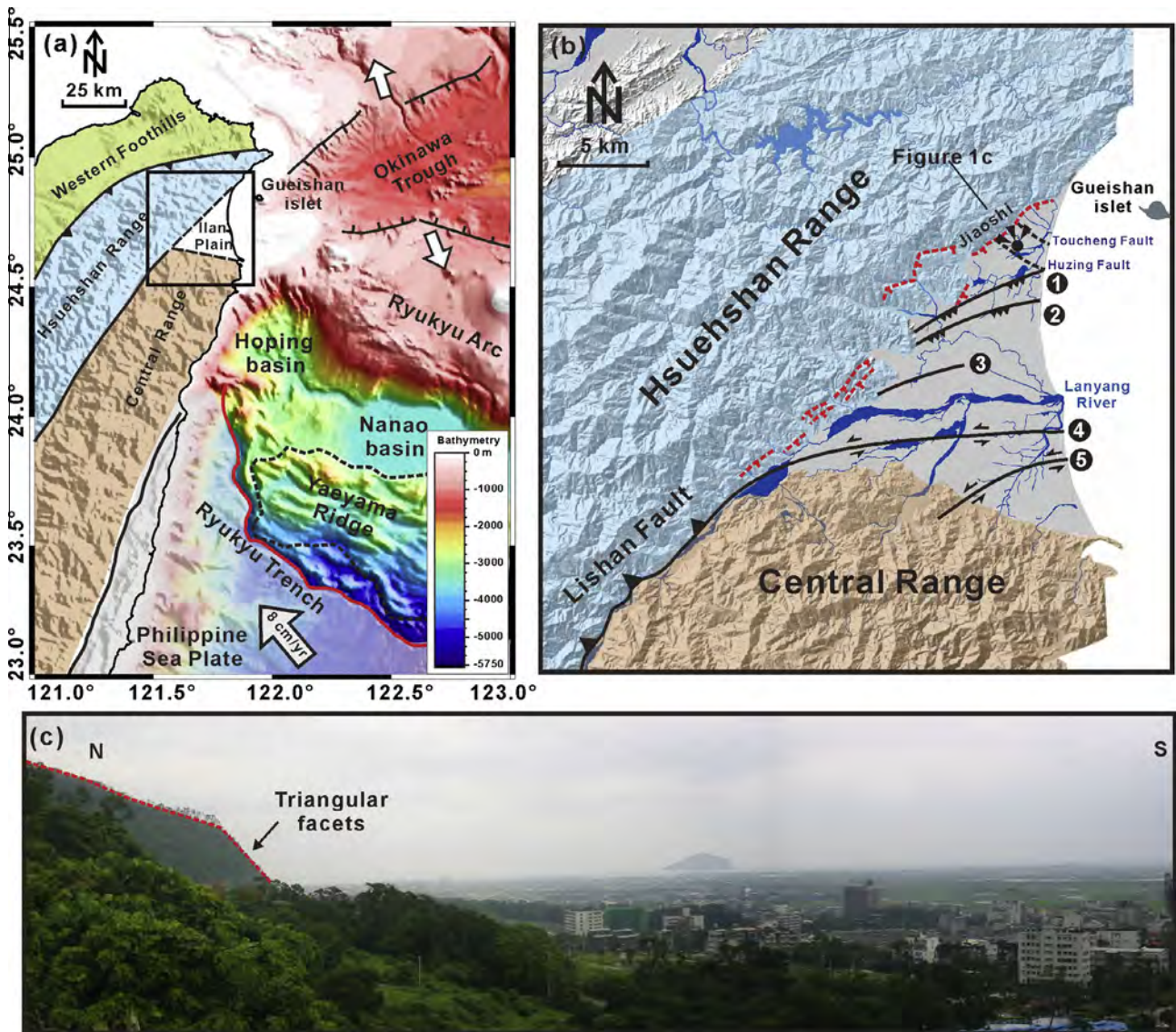
1. Introduction

In regions with active tectonics, identification and characteriza-tion of surface deformations are generally based on geomorphic and structural analyses using satellite images or aerial pho-tographs combined with digital elevation model (DEM) at different spatial scales, as well as with field observations. Using these approaches, the regional pattern of surface deformation can be compared to fault kinematics (from offset of geomorphic features or fault slip vectors), the earthquakes distribution (instrumental and historical seismicity), and mechanisms of focal solutions. However, in extensional settings, high subsidence rates may induce overlaid deposition, erasing the geomorphic features tradi-tionally used to localize active deformation. Within such tectonic

frameworks, remote sensing analyses using Interferometric Synthetic Aperture Radar (InSAR) techniques are well suited to determine the deformation pattern related to fault activity (Zebker et al., 1994; Massonnet and Feigl, 1998; Chang et al., 2004).

Located at the boundary between the Eurasian and Philippine Sea plates, Taiwan is an ideal location to address major questions regarding lithospheric deformation mechanisms in convergent set-tings, mountain building processes from oceanic subduction to continental subduction, and post orogenic extension (Fig. 1a). In this paper, we focused on the recent deformation of the Ilan Plain in northeast Taiwan. The formation of the Ilan Plain is often related to the opening of the Okinawa Trough (Ho, 1986; Tsai, 1986), the back-arc basin of the Ryukyu subduction system (Teng, 1990) (Fig. 1a). Indeed, the Ilan Plain is generally described as bounded by normal faults to northwest, where subdued triangu-lar facets can be depicted from the morphology (Lee and Wang, 1988; Shyu et al., 2005) (Fig. 1b and c). However, due to a combi-nation of both high subsidence and deposition rates, geomorphic evidences of fault activity, like cumulated fault escarpments, can-not be observed in the late Quaternary deposits that spread onto

* Corresponding author at: Center for Space and Remote Sensing Research, National Central University, 300 Jhongda Rd., Jhongli City, Taoyuan County 320, Taiwan. Tel.: +886 3 4227151x57671.

E-mail addresses: chuchun@earth.sinica.edu.tw (C.-C. Kang), cpchang@csrsr.ncu.edu.tw (C.-P. Chang), siame@cerege.fr (L. Siame), jclee@earth.sinica.edu.tw (J.-C. Lee).

Fig. 1. (a) Tectonic framework and main structural units of the northeastern Taiwan mountain belt and its connections to the Okinawa Trough back-arc basin and Ryukyu arc, accretionary wedge, and trench subduction systems. The plate convergence of the Philippine Sea plate relative to Eurasia is ongoing at a rate of roughly 82 mm/yr in a northwest direction (Yu et al., 1997; Sella et al., 2002). Bathymetry data are from Sibuet et al. (1998). (b) The Ilan Plain is triangular in shape and is bordered by the Hsuehshan Range to the north and west and the Central Range to the south and east. Bounding subdued normal faults are shown with red dotted lines after Shyu et al. (2005). Buried faults marked by dashed black lines are after Jhiang (1976): (1) the Yaichein Fault; (2) Ilan Fault; (3) Kengssu Fault; (4) Choshui Fault; and (5) Sansing Fault. (c) Field photograph looking NE at Jiaoshi showing the subdued triangular facets along the Hsuehshan Range. (For interpretation of the references to colour in this figure legend, the reader is referred to the web version of this article.)

the Ilan Plain at the toe of the Hsuehshan and Central ranges. To the south of the plain, the mountain front is even more sinuous, showing little evidence for localized normal faulting deformation. In fact, the extensional nature of the Ilan Plain region is supported by the pattern of active deformation determined from seismicity and geodetic measurements (e.g., Hu et al., 1996; Rau et al., 2008; Kang et al., 2008; Angelier et al., 2009; Ching et al., 2011b; Huang et al., 2012). In this paper, we applied the Persistent Scatterer Interferometric Synthetic Aperture Radar (PSI) technique, which allows measuring the surface deformation rate and addressing the decorrelation and atmospheric problems underlying conventional radar interferometry approaches (Hooper et al., 2004, 2007; Hooper, 2008). After presenting the geological setting of the Ilan Plain, and the PSI results for this area, we compare our data with previous geodetic surveys and discuss the relationships between the observed pattern of surface deformation and the distribution of basement structures in connection with the Okinawa Trough.

2. Geological setting of the Ilan Plain

The Ilan Plain is a triangular, deltaic plain characterized by flat topography and elevation close to sea level. It is surrounded by the high mountains of the Hsuehshan Range to the northwest and the Central Range to the south. Its eastern coast faces the western tip of the Okinawa Trough (Fig. 1). The Ilan Plain is fed by the Lanyang River, the second largest river in northern Taiwan (Fig. 1b), which discharges nearly 10 million tons of sediment per year into the Okinawa Trough (Liu et al., 2006).

Fault identification under the Ilan Plain is an important key to demonstrate the Ilan Plain as the western elongation of the southwestern propagation of the Okinawa Trough (Jhiang, 1976; Liu, 1995; Liang et al., 2005; Kang et al., 2008; Angelier et al., 2009; Hou et al., 2009). Most of these studies considered the Ilan Plain as the western elongation of the southwestern propagation of the Okinawa Trough (e.g., Teng, 1990). Using seismic reflection profiles,

the pioneer work by Jhiang (1976) identified a series of faults buried below the alluvial deposits of the Ilan Plain and rooting at depth within the Central Range and Hsuehshan Range rock formations (Fig. 1). These faults were previously regarded as inactive thrust faults from the tectonic regime during collision and mountain building. However, considering the active tectonics of the Ilan Plain (e.g., Kang et al., 2008; Angelier et al., 2009), some of these faults may actually play a key role during the tectonic inversion from compressive to extensional deformation that is suspected to occur in connection with the opening and propagation of the Okinawa Trough (e.g., Ho, 1986; Tsai, 1986).

In the Ilan Plain, strong impact of erosional and depositional processes on the landscape precludes recording long-term deformation by geomorphic features. Previous studies thus mostly relied on geodetic (Global Positioning System (GPS), leveling) and seismological observations. From a 10-years long leveling survey, Liu (1995) determined a rapid subsidence rate of ~20 mm/yr between Ilan and Loudung cities combined with an eastward tilting of the plain of approximately 0.44 μradian/yr. Based on GPS measurements, Hou et al. (2009) showed that the Ilan Plain is moving to the southeast (N143°E) at a maximum rate of ~43 mm/yr (Fig. 2). Regional geodetic measurements and seismological analyses, suggested that the surface deformation pattern of the Ilan Plain might be affected by the active Choushui Fault (Fig. 2), with the southern half of the plain undergoing clockwise rotation (Rau et al., 2008; Angelier et al., 2009; Ching et al., 2011b). Using GPS-derived strain tensors, which indicate horizontal deformation and three-dimensional stress regimes determined from inversion of earthquake focal mechanisms, these authors proposed a tectonic pattern for the Ilan Plain involving a non-rigid, clockwise rotation,

with transition from pure compression near mountains to transtension near the sea (Fig. 2). This tectonic pattern is consistent with a northwest oriented, left-lateral simple shear affecting the deforming domain (Liang et al., 2005) and reflects the lateral extrusion of the Ilan Plain towards the Ryukyu subduction zone, which acts as a mechanically weak domain with respect to the collision zone (Angelier et al., 2009). However, this regional pattern of surface deformation might have been influenced by the surface deformation associated by the earthquake sequence that occurred in 2005. More recently, Ching et al. (2011b) used leveling and continuous GPS observations (2000–2008) and compared them to the long-term rates of subsidence derived from boreholes and showed that they are comparable (5–10 mm/yr) in the northern half of the plain whereas the geodetic rates appear two times faster (roughly 20 mm/yr) in the southern half of the plain, suggesting a recent southward migration to the subsidence center.

Previous studies have yielded significant knowledge on the deformation mechanics of the Ilan region, with the identification of a main active structure, the Choushui fault, which appears to be inverted from the pre-existing major thrust between the Hsuehshan Range and the Central Range in the middle of the plain (Rau et al., 2008; Kang et al., 2008). However, its surface expression is still unclear and existence of other active structures remains debatable (e.g., Angelier et al., 2009). Identifying and characterizing those structures is thus an important step in evaluating their seismogenic potential and associated seismic hazards for the populated Ilan region.

In the Ilan Plain, the background seismicity exhibits a significant E-trending zone of activity south of the Lanyang River (Huang et al., 2012). In our opinion, the coincidence of a high
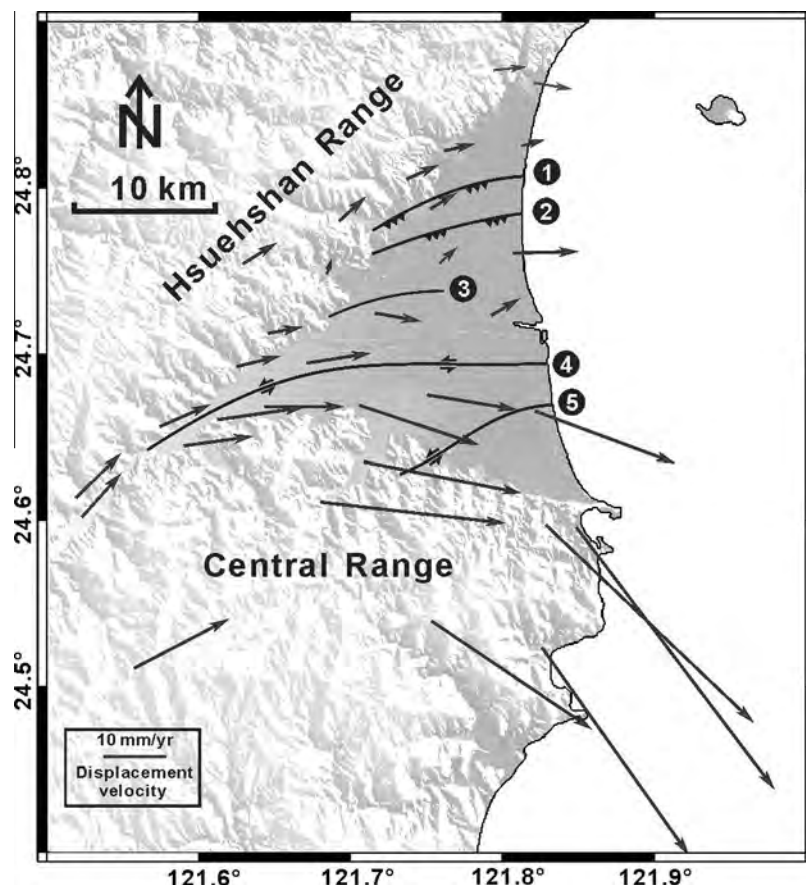

Fig. 2. Horizontal velocity field of GPS stations in Ilan Plain relative the Penghu Islands, located in the Taiwan Strait (Hou et al., 2009). Fault lines (black lines) are after Jhiang (1976) (see also Fig. 1).

subsidence area with such a seismic swarm may be representative of movements localised at depth on faults below the Plio-Quaternary deposits of the Ilan Plain. On May 15, 2002 and March 5, 2005, two main earthquakes occurred in the south of the Ilan Plain offshore area, the focal mechanisms are left-lateral strike-slip faulting and lateral extrusion at the transition between Taiwan mountain range and Okinawa Through (Liang et al., 2005; Huang et al., 2012).

To determine the pattern of surface deformation of the Ilan Plain in more detail, we used the PSI technique to decipher the regional pattern of deformation rates and compared it to other existing geophysical data (Liu, 1995; Hsu, 2006; Rau et al., 2008; Chiu et al., 2008; Hou et al., 2009; Ching et al., 2011b). Our results allow identifying a zone of high subsidence located in the southern part of the Ilan Plain, and discussing how far it is correlated to the lateral extrusion of the Central Range in connection to back-arc

opening associated with the southward retreat of Ryukyu Trench (e.g., Rau et al., 2008; Angelier et al., 2009; Lallemand et al., 2013).

3. Persistent Scatterer InSAR in the Ilan Plain

### 3.1. Methodology and data acquisition

Persistent Scatterers (PS) are ground points of radar images characterized by interferometric phase behavior that is stable over time for wide look-angle variations (i.e., buildings or non-vegetated areas, which have high long-term phase coherence and a strong and stable backscatter level). This characteristic overcomes the decorrelation issue underlying conventional radar interferometry technique (Ferretti et al., 2001; Hooper, 2008). Given the spatially and temporally consistent atmospheric contributions, the main goal of PSI processing is to separate the surface deformation from overall spatial–temporal changes in radar images, including atmospheric delay anomaly, DEM error, orbit error, and decorrelation noise, by means of least-square estimations and iterations. This approach considers the spatial and temporal distributions as well as the correlation between PS pixels. After removing errors due to atmospheric anomaly, orbit and DEM effects at each PS point the surface deformation can be determined with millimeter scale precision. The PSI technique has previously been applied successfully to monitor and estimate landslides, urban subsidence, and deformation associated with tectonic and volcanic processes (Bürgmann et al., 2000; Hooper et al., 2007; Massironi et al., 2009). During the past years, Hooper et al. (2004) and Hooper (2008) have developed a new PS analysis method, called StaMPS (Stanford Method for Persistent Scatterer), to extract the deformation signal in regions with no bright scatterers and areas undergoing non-steady deformation. No prior knowledge of deformation rate variations is needed for this approach, which has already been applied successfully to the Taipei Basin in Taiwan, allowing determination of uplift and subsidence areas that are in good agreement with leveling data (Chang et al., 2010).

In this study, we applied Hooper's (2008) method to identify PS pixels and estimate deformation of the Ilan Plain by using 23 ENVISAT scenes acquired between 2004 and 2008 along descending orbits (Table 1 and Fig. 3). This series of scenes resulted in 28,790 PS points being retained and selected, which typically correspond to man-made structures (e.g., buildings, poles, and antennas). Considering the baseline condition and time span, we chose the image of 26th November 2005 as the master image, which has the maximum perpendicular baseline of 519 m.

Table 1
Parameters of ENVISAT-SAR images used for PSI analysis. The master image is fixed on 26th November 2005. From 2004 to 2008, information on the slave images of each pair, including date of acquisition, interval time, and perpendicular baseline ($B_\perp$) with the master image are given in this table. Track = 461, frame = 3105.

Pair	Date	Orbit	$B_\perp$ (m)	Days
1	20040306	10535	55	−630
2	20040515	11537	−217	−560
3	20040619	12038	104	−525
4	20040724	12539	383	−490
5	20040828	13040	68	−455
6	20041002	13541	−12	−420
7	20041106	14042	76	−385
8	20041211	14543	−138	−350
9	20050604	17048	−289	−175
10	20050813	18050	−310	−105
11	20050917	18551	333	−70
Master image	20051126	19553	0	0
12	20060902	23561	519	280
13	20061007	24062	− 418	315
14	20070120	25565	460	420
15	20070224	26066	204	455
16	20070331	26567	355	490
17	20070609	27569	24	560
18	20070714	28070	18	595
19	20071201	30074	248	735
20	20080105	30575	− 328	770
21	20080209	31076	249	805
22	20080628	33080	156	945
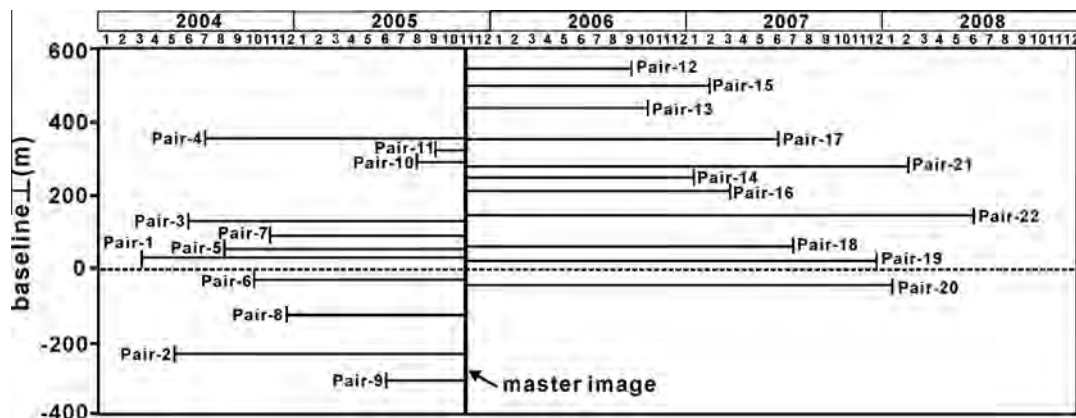
Fig. 3. Image pairs used for PSI analysis. The ENVISAT satellite in the descending orbit track 461, frame 3105, has acquired all the images. Cross axis indicates acquisition time; vertical axis and number in parentheses show perpendicular baselines in meters. Considering the baseline condition and time span, the master image is fixed on 26th November 2005. The maximum perpendicular baseline is 519 m (pair-12). Detailed parameters are given in Table 1.

3.2. Results

Fig. 4 shows the unwrapped phase of PS pixels for each image referenced to the master image. In these interferograms, a 40-m resolution DEM was applied to remove topographic effects. However, the residual phases shown in Fig. 4 still contain errors from other sources, such as atmospheric retardation, orbit inaccuracies, DEM error, and noise (variability in scattering, thermal noise and co-registration errors). Selected PS pixels being defined where the noise value is the smallest; this latter component can be neglected. The phase error resulting from DEM uncertainty can be corrected by using precise orbit data (Fig. 5a) (Hooper et al., 2004). Once corrected for DEM uncertainty, the corrected phase values can be unwrapped, but the resulting interferograms still contain atmospheric and orbit errors. The spatially correlated errors can be estimated by filtering the unwrapped data in time (high-pass filter) and in space (low-pass filter) (Ferretti et al., 2001). The resulting signal (i.e., atmospheric and orbit error of the master image) can be subtracted from the interferograms, leaving only the phase change due to pixel movement in the line-of-sight (LOS) direction of satellite radar. After removing the DEM, atmospheric, and orbit errors, the image resulting from the stacking of all of the interferograms can be regarded as the slant range displacement rate between the PS points and the satellite (Fig. 5b). The standard deviations of the velocity field present a twofold pattern with rather uniform and small values (<0.4 mm/yr) in the

plain area, and more variable and higher values (2–3 mm/yr) in the reliefs (Hsuehshan Range and Central Range) that may be attributed to the dense vegetation in the mountain areas (Fig. 5c). Since displacement rates derived from PSI represent slant range relative offsets of the PS pixels respect to neighboring areas, an adjusted displacement field has thus been determined using the most stable point along leveling routes (control point) over the last 10 yrs as reference point (Fig. 6a). This allows comparison of the results of our PSI with existing previous geodetic surveys, such as GPS and leveling data. In the study area, the relative horizontal displacement is small, so the shortening and elongation in slant range are mainly caused by land uplift and subsidence, respectively.

The derived pattern of slant range displacement in the Ilan Plain shows high-level of present-day (2004–2008) subsidence localized in the southern part of the plain, south of the Lanyang River (Fig. 6a). In this part of the plain, the subsidence rate ranges from 10 to 18 mm/yr over the 4 yrs of observation (Fig. 6a). On the other hand, the central part of the Ilan Plain, north of the Lanyang River and east of Ilan city, is also subsiding but at a lower rate of 2–8 mm/yr (Fig. 6a).

Land subsidence can be strongly influenced by human activity, such as the pumping of ground water for fishponds or agriculture activities causing dewatering of sediments (Hsieh et al., 2011). In order to check for possible dewatering effects within our study area, we compared the location of pumping areas and water table fluctuation of 6 wells (Fig. 6a and b) to our PSI results. According to
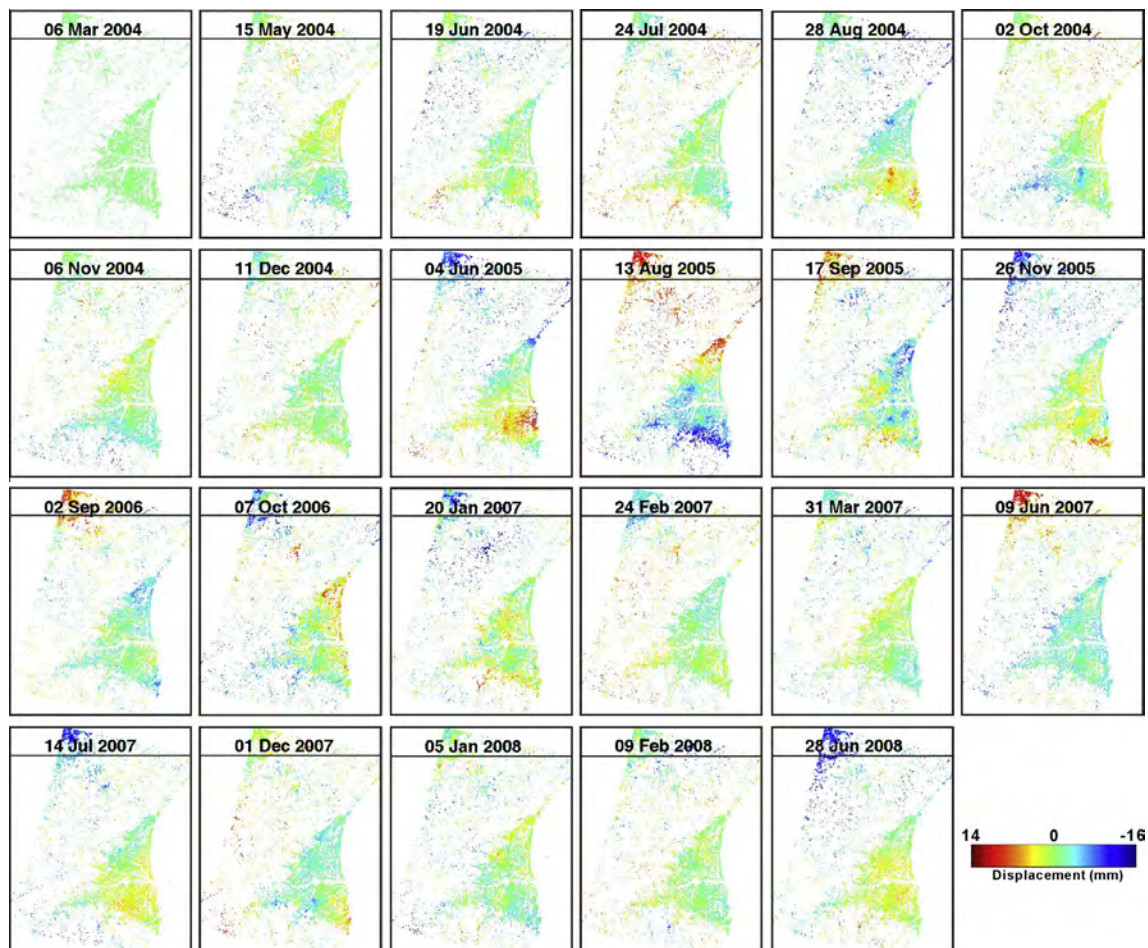

Fig. 4. Unwrapped phase of PS pixels of each image referenced to the master image. Time interval and perpendicular baseline are shown in Fig. 3. The positive value in reddish color represents shortening, and the negative value in bluish color represents elongation along the line of sight (LOS) direction compared to the master image. (For interpretation of the references to color in this figure legend, the reader is referred to the web version of this article.)
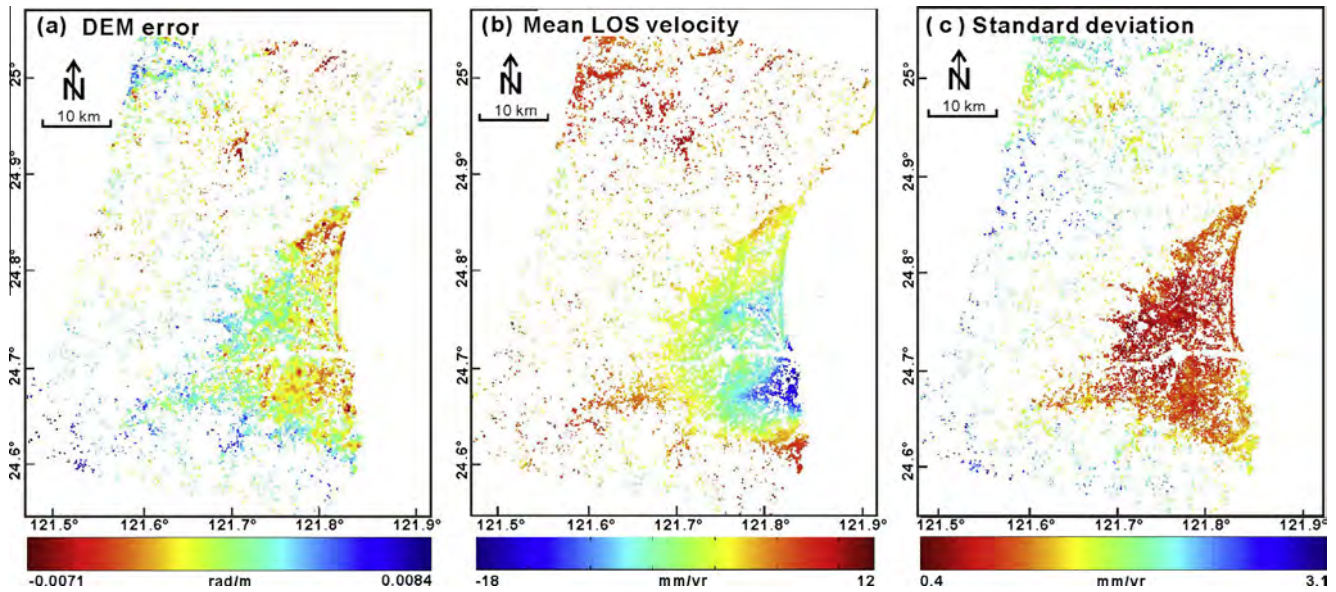
Fig. 5. (a) Estimated digital elevation model (DEM) error of the master image. (b) The unwrapped residual phase result of PS pixels. Because the errors in (a) have been removed, this image can be considered as the map of slant range displacement rates between the PS and satellite. The positive value in reddish color represents shortening, and the negative value in bluish color represents elongation along the radar LOS during the observation period (2004–2008). (c) The standard deviation of the Mean LOS velocity field. (For interpretation of the references to color in this figure legend, the reader is referred to the web version of this article.)

these data, the fluctuations of water tables, though showing seasonal variations for number 2, 3, 4, and 5 of the wells, are 4–10 times smaller than the PSI-derived subsidence rates during the observation period (2004–2007). This implies that water-pumping activities cannot be regarded as responsible for the observed subsidence pattern. Conversely, the area south of the Lanyang River where the subsidence in max is also characterized by occurrence of the major and most shallow seismic events (*e.g.*, the 2005 two M5.9 earthquakes doublet) during the time span encompassed by the ENVISAT time series (Fig. 6a), suggesting that it may have a close relationship with tectonics.

4. Discussion

4.1. Comparison with previous geodetic surveys

In the Ilan Plain, surface deformation has been previously surveyed using GPS (Yu et al., 1997; Rau et al., 2008; Hou et al., 2009; Hsu, 2006; Chiu et al., 2008; Ching et al., 2011b) and leveling (Liu, 1995; Ching et al., 2011a; Water Resources Agency, Ministry of Economic Affairs) techniques. The GPS surveys of the Ilan Plain covered a variety of different periods from 1995 to 2008. The leveling surveys were conducted from 1985 to 1994 (Liu, 1995) and from March 2002 to August 2007 (Water Resources Agency, 2015). We selected 7 continuous GPS (CWB and IES) and leveling (Water Resources Agency, 2015) data sets that encompass the time span of the PSI data used in this study. There is a strong discrepancy between the spatial resolutions of these different techniques (>28,000 PSI points *vs.* 7 GPS and 31 leveling stations). However, to allow straightforward comparison, the 3-D continuous GPS data were projected onto the LOS of the ENVISAT radar, and interpolated with a resolution of 2.5 km (Fig. 6c). Due to their limited number and individual poor vertical resolution, each GPS station may significantly weight in the regional pattern derived from their spatial interpolation.

At a first order, both PSI- and GPS-derived patterns of LOS displacement are comparable and shows that the highest subsidence rates are located in the southern part of the Ilan Plain (Fig. 6). For example, in the area located to the east of Loudung city, south of

the Lanyang River, both data sets exhibit a high level of subsidence rate ranging from 14 to 18 mm/yr (Fig. 6a and c). In addition, the PSI data are also consistent with the vertical movements derived from leveling surveys measured along the coast of the Ilan Plain (Fig. 6d; Water Resources Agency, 2007). South of the Lanyang River, both datasets indicate that the Ilan Plain is subsiding at a maximum rate of 18 mm/yr. North of the Lanyang River, they indicate the same trend, although the PSI-derived vertical rates are slightly slower than the leveling-derived rates (Fig. 6d). This discrepancy might be due to the horizontal displacement, which is also included in the PSI results but cannot be depicted from the leveling measurements. Even if they differ from their spatial resolution, the GPS and leveling surveys are in good agreement with the PSI data, suggesting that this late dataset provides a high-resolution subsidence distribution map for the Ilan Plain.

4.2. Relationships between surface deformation and basement structures

A key issue is the relationship between the observed PSI-derived surface displacements and the structural framework of the basement below the thick Quaternary deposits of the Ilan Plain. Indeed, active faults responsible for this surface deformation may be potential sources of seismic hazard that deserve attention through examination of existing geophysical data and the distribution of crustal seismicity over the same period than the PSI time series.

Jhiang (1976) used shallow seismic reflection profiles and boreholes data to determine the geometry of the Tertiary basement below the Quaternary sediments of the Ilan Plain. This pioneer study revealed that the roof of the Tertiary basement is deeper (up to 1499 m) near the Hsuehshan Range than it is south of the Lanyang River (200–600 m). The area of high subsidence revealed by our PSI approach is thus not coincident with the Quaternary depocenter but shifted to the south of the Lanyang River (Fig. 7a). Jhiang (1976) also delineated the major faults structuring the basement below the Quaternary deposits (Fig. 7a). It is worth noting that the area with the highest subsidence rates derived from PSI data is located near the Choshui Fault (fault number 4 in
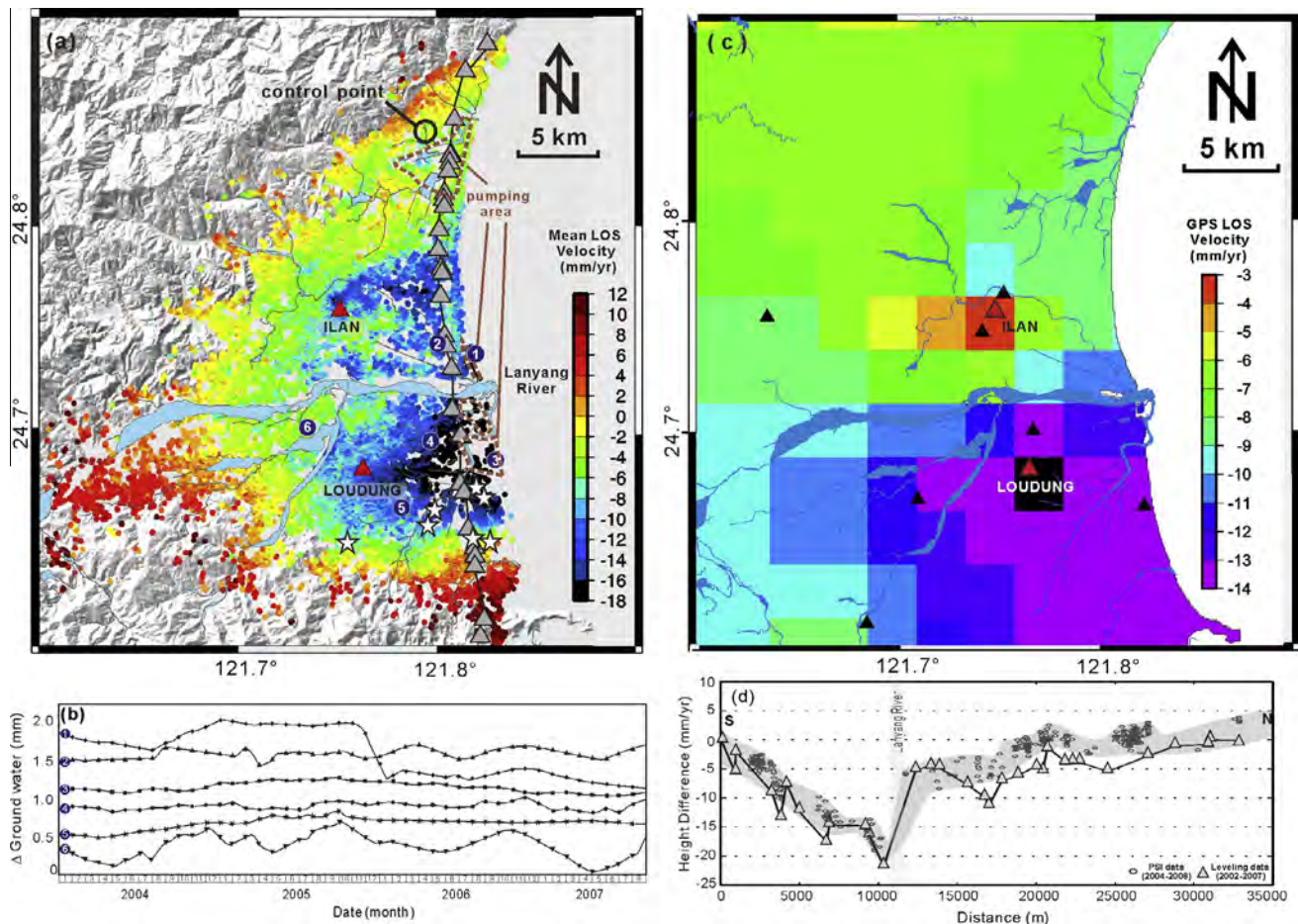
Fig. 6. (a) Mean LOS ground velocity derived from PS InSAR in the Ilan Plain. The results have been adjusted using a leveling point (fixed pixel) relatively stable over the last 10 yrs (data from Water Resources Agency, Ministry of Economic Affairs). Topographic map in the background is the Taiwan digital elevation model from the Taiwan Forestry Bureau (40-m resolution). The positive values (reddish color) represent shortening and the negative values (bluish color) represent elongation along the radar LOS during the observation period (2004–2008). The areas delineated by brown dotted lines represent zones of groundwater pumping (e.g., fish farms). Open stars locate seismic events with focal depths above 15 km and magnitudes larger than 4 (2004–2008, Earthquake catalog of Central Weather Bureau). The blue circles represent the location of water wells (2004–2008, Water Resources Agency, Ministry of Economic Affairs). (b) Ground water hydrographs recording aquifer levels measured within wells (Water Resources Agency, Ministry of Economic Affairs), and showing the low seasonal impacts of water pumping on aquifers since water levels do not decline during summer while water demands increase. (c) Interpolated map of GPS-derived displacement rates in the radar LOS direction (data from CWB and IES). (d) Plot showing the vertical movements along the leveling line in the Ilan Plain during the period from 2002 to 2007 (data from Water Resources Agency, Ministry of Economic Affairs). PSI data are shown with black circles and leveling points with gray triangles. (For interpretation of the references to color in this figure legend, the reader is referred to the web version of this article.)

Fig. 7a) where the earthquake distribution also shows a high-level of seismic activity. Lai et al. (2009)'s relocated epicentre distribution for the 2005 earthquake sequence locates this seismic activity south of the Choshui Fault and in the vicinity of the Sansing Fault projected at the surface. As far as Jhiang (1976) seismic profile interpretation is concerned, the basement faults in the southern part of the Ilan Plain are dipping to the south. Thus, if the PSI-derived subsidence is controlled by fault activity, the Choshui Fault could be regarded as the master fault. Actually, most of the focal mechanisms recorded between 2004 and 2008 are characterized by strike-slip (left-lateral) movements with normal component that are in good agreement with the ground displacement pattern derived from the PSI data (Fig. 7). However, the focal mechanisms (with focal depths above 50 km) from 2004 to 2008 earthquake sequences apparently distribute along a steep angle fault plane, which is different from that of the presumable S-dipping Choushui Fault (e.g., Jhiang, 1976). Furthermore, According to the double earthquake event on 2005 March 5, the focal mechanisms are strike-slip faults with some normal component (Lai et al., 2009) (Fig. 7b). In our opinion, the coincidence of this high subsidence area with such a seismic activity may be

representative for active normal structure below the Quaternary deposits of the Ilan Plain, in good agreement with Lai et al. (2009) and Tong et al. (2008)'s dyke injection interpretations in relation with fault activity at depth. One end-member hypothesis would be to associate this earthquake sequence with the south-dipping Choshui Fault, in agreement with the relocated main shocks from the 2005 double earthquake (Lai et al., 2009).

To evaluate the extent to which the PSI-derived subsidence pattern is influenced by surface deformation induced by this earthquake sequence, we used Okada (1985) approach to simulate the surface deformation due to a dislocation in an elastic half-space. The theoretical dislocation is located along the Choshui Fault and the fault model parameters are those proposed by Lai et al. (2009). To make the simulated ground deformation comparable with the PSI-derived subsidence pattern, the dislocation results were projected onto the LOS of the ENVISAT radar, and interpolated with a resolution of 3 km (Fig. 8). Within the framework of this hypothesis, the simulated ground displacement is in good agreement with the subsidence pattern and suggests that up to 40% of the LOS surface displacement could be related to the 2005 earthquake sequence. Even if it is still speculative to attribute the
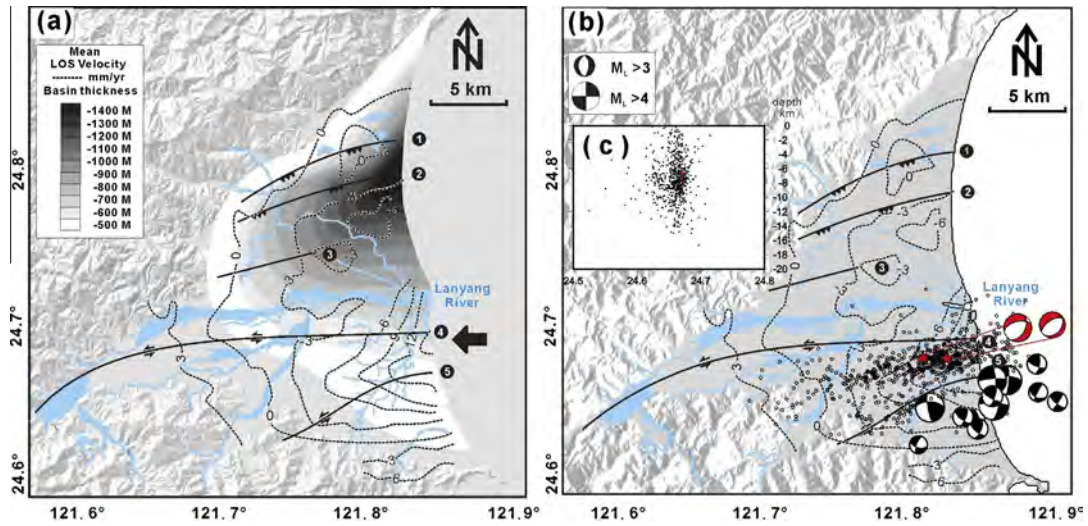
Fig. 7. (a) Map of the Plio-Quaternary basin thickness in the Ilan Plain (after Jhiang, 1976). Black dashed lines show the PSI mean LOS velocity contours, and the black arrow highlights the area with the highest subsidence rate. Black solid lines show the fault traces in the Ilan Plain as mapped by Jhiang (1976). (b) Focal mechanisms distribution during 2004–2008 with focal depths above 50 km (Broadband Array in Taiwan for Seismology). Open stars locate seismic events (Lai et al., 2009). Red beach-balls represent the first-polarity focal mechanisms by Lai et al., 2009. (c) N–S cross-section of projected hypocenters. The main hypocenter swarm suggests an active structure dipping to the south (hypocenters relocated by Lai et al., 2009). (For interpretation of the references to color in this figure legend, the reader is referred to the web version of this article.)
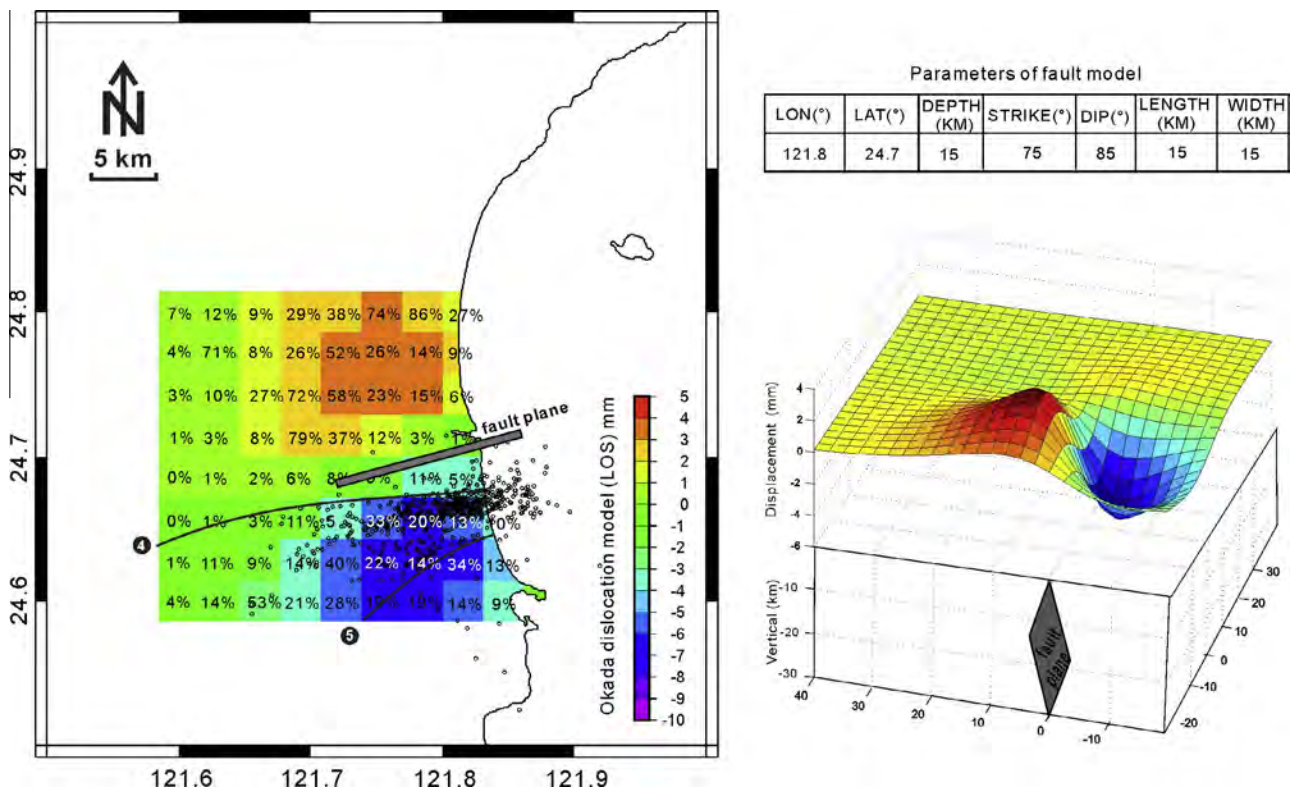

Fig. 8. Simulated surface deformation based on the dislocation model in an elastic half-space (after Okada, 1985). The results were projected onto the LOS of the ENVISAT radar and interpolated with a resolution of 3 km. The fault plane parameters have been modeled by Lai et al., 2009.

responsibility of the observed subsidence pattern to a particular fault like the Choshui Fault, it seems rather clear that a significant part of the signal could be associated to tectonic activity. Within the southern part of the Ilan Plain, the high subsidence rate might well also be the cause of the opening of back-arc basin as a whole, allowing for dyke injections, as suggested by Tong et al. (2008) and Lai et al. (2009), and sediment compaction as described by Cheng and Hong (2012).

In the Ilan Plain, the deepest basement is located in the northern part close to the Hsuehshan Range (Fig. 9), which implies that this area has accumulated the largest amount of long-term subsidence during Quaternary. Generally, in the recent sedimentary basin with thick deposit, the surface subsidence caused by compaction is faster. In our study case, the thickest deposit is in the northern part, the most recent deposit is in the central part, but the most rapid subsidence occurs in the southern part of the Ilan
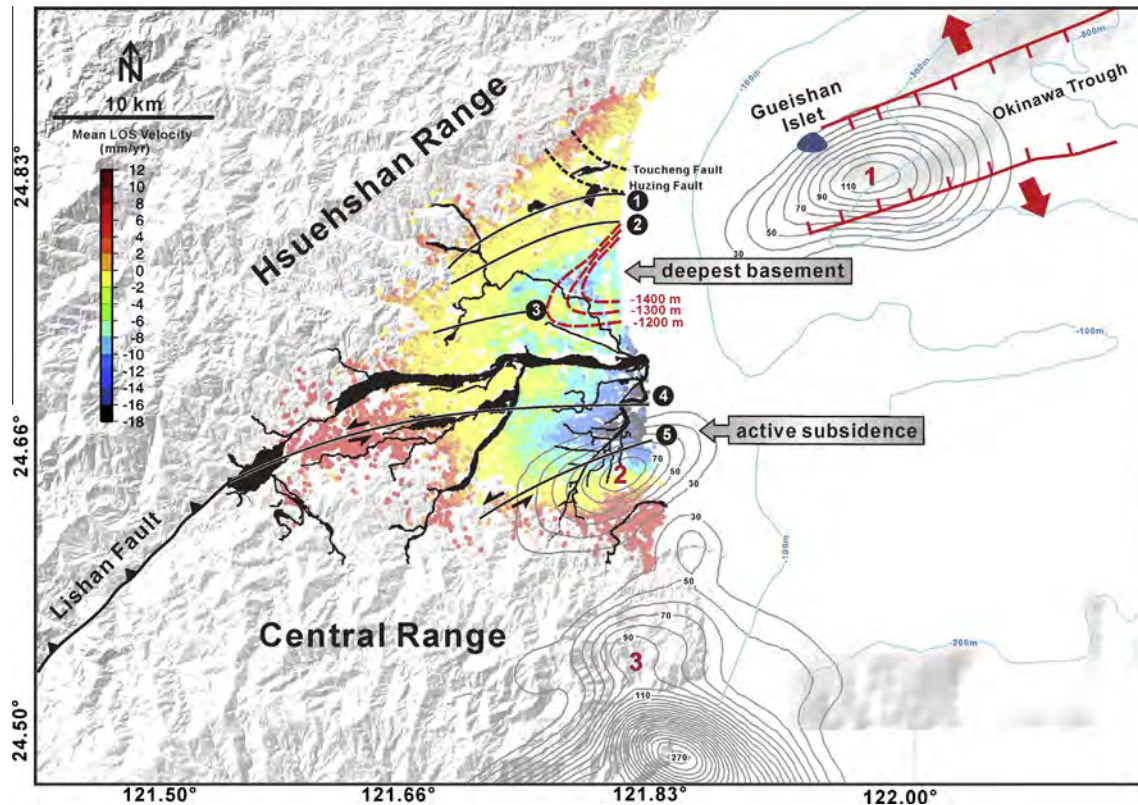
Fig. 9. Map of the Ilan Plain showing LOS displacement of PSI during the period of 2004–2008. Black dashed lines correspond to basement faults from seismic data after Jhiang (1976) and modified in the northern part according to Shyu et al. (2005). The colored points are the mean LOS velocity of the processed PS (same legend as for Fig. 6a). Topographic map in the background is the Taiwan digital elevation model from the Taiwan Forestry Bureau (40 m resolution). Gray contour lines represent the earthquake density distribution (1973–2008, Central Weather Bureau Earthquake Catalog) with depth above 30 km and no magnitude cut-off. These contour lines have been obtained by gridding the number of events with a cell-resolution of 0.5 km. This distribution map clearly shows the seismicity patches in areas where the seismicity is related (1) to the opening of the Okinawa Trough, (2) to the Sansing Fault, and (3) to the collision zone in the Hualien area. Red dotted lines show the depth of the basement roof (after Jhiang, 1976) and thus illustrate the Plio-quaternary depocenter. (For interpretation of the references to color in this figure legend, the reader is referred to the web version of this article.)

Plain. We thus believe that the tectonic process plays an important role for this subsidence. Another point is the direction of the Lanyang River when it flows through the Ilan Plain. Actually, the riverbed of this major river is not following the Quaternary depocenter but rather seems to be diverted southwardly to reach the sea close to the high subsidence area (Fig. 9). Together with the data and observations regarding PSI, GPS, leveling and seismicity activity, this strongly suggests that the propagation of the Okinawa Trough through the Northern part of the Taiwan orogen lead to the southward migration of the basin depocenter (Fig. 9).

5. Conclusions

In the Ilan Plain, the tectonic pattern is complex and reflects lateral extrusion toward a mechanically weak domain with respect to the collision zone; that is, the adjacent Ryukyu subduction zone (e.g., Angelier et al., 2009). This region has been investigated by considering horizontal displacement revealed by recent geodetic surveys (Hou et al., 2009; Ching et al., 2011b) and derived strain rate tensors, indicating horizontal deformation and 3-D seismotectonic stress regimes from inversion of earthquake focal mechanisms (Angelier et al., 2009). In this paper, this complex tectonic setting has been investigated using a PSI approach, providing a high-resolution subsidence map (Fig. 6a). A high subsidence area located south of the Lanyang River and not directly above the main Quaternary depocentre (e.g., Jhiang, 1976) is thus depicted, and strongly favors an opening of the basin directed to the south. In

addition, the remarkable correlation between crustal seismicity and subsidence rate also suggests that this area is most likely connected to the activity of basement faults below the Quaternary deposits.

If these converging pieces of evidence are true, then the seismic swarm may be the best candidates for explaining the observed surface deformation pattern. Indeed, seismic activity occurs between the Choshui Fault and the front of the Central Range, along the northern elongation of Sansing Fault (Fig. 9). According to scaling laws for strike-slip faults, such a range of subsurface lengths suggests Mw ranging from 6.1 to 6.3 (Wells and Coppersmith, 1994). In March 2005, a cluster of earthquakes with maximum magnitude of 5.8 occurred in this area, similar to the lower bond estimated from scaling laws. It is not known how far these structures continue offshore, so the Mw values determined from scaling laws should be regarded as minimal estimates. This uncertainty reinforces the idea that these structures should be considered as important sources of seismic hazards for the Ilan Plain population and infrastructures and thus requires further investigations.

References

Angelier, J., Chang, T.Y., Hu, J.C., Chang, C.P., Lionel, S., Lee, J.C., Deffontaines, B., Chu, H.T., Lu, C.Y., 2009. Does extrusion occurs at both tips of the Taiwan collision belt? Insights from active deformation studies in the Ilan Plain and Pingtung plain regions. Tectonophysics 466, 356–376.

Bürgmann, R., Rosen, P.A., Fielding, E.J., 2000. Synthetic aperture radar interferometry to measure Earth's surface topography and its deformation. Ann. Rev. Earth Planet. Sci. 28, 169–209.

Chang, C.P., Wang, C.T., Chang, T.Y., Chen, K.S., Liang, L.S., Pathier, E., Angelier, J., 2004. Application of SAR interferometry to a large thrusting deformation: the 1999 Mw = 7.6 Chichi earthquake in Central Taiwan. Geophys. J. Int. 159, 9–16.

Chang, C.P., Yen, J.Y., Hooper, A., Chou, F.M., Chen, Y.A., Hou, C.S., Hung, W.C., Lin, M.S., 2010. Monitoring of surface deformation in northern Taiwan using DInSAR and PSInSAR techniques. Terr. Atmos. Ocean. Sci. 21, 447–461.

Cheng, Y.C., Hong E, 2012. The paleo environment analysis of the Ilan Plain. Western Pacific Earth Sci., 12(2) (accepted for publication).

Ching, K.E., Rou, R.J., Johnson, K.M., Lee, J.C., Hu, J.C., 2011a. Present-day kinematics of active mountain building in Taiwan from GPS observations during 1995– 2005. J. Geophys. Res. 116, B09405. http://dx.doi.org/10.1029/2010JB008058.

Ching, K.E., Hsieh, M.L., Johnson, K.M., Chen, K.H., Rau, R.J., Yang, M., 2011b. Modern vertical deformation rates and mountain building in Taiwan from precise leveling and continuous GPS observations, 2000–2008. J. Geophys. Res. 116, B08406. http://dx.doi.org/10.1029/2011JB008242.

Chiu, Y.T., Ching, K.E., Hou, C.S., Hu, J.C., Rou, R.J., 2008. Crustal deformation of Ilan Plain from GPS observations, 2002–2006. Spec. Publ. Central Geol. Survey 20, 111–124.

Ferretti, A., Prati, C., Rocca, F., 2001. Permanent scatteres in sar interferometry. IEEE Trans. Geosci. Rem. Sens. 39 (1), 8–20.

Ho, C.S., 1986. A synthesis of the geological evolution of Taiwan. Tectonophysics 125, 1–16.

Hooper, A., 2008. A multi-temporal InSAR method incorporating both persistent scatterer and small baseline approach. Geophys. Res. Lett. 35, L16302. http:// dx.doi.org/10.1029/2008GL034654.

Hooper, A., Zebker, H., Segall, P., Kampes, B., 2004. A new method for measuring deformation on volcanoes and other natural terrains using InSAR persistent scatterers. Geophys. Res. Lett. 31, L23611. http://dx.doi.org/10.1029/ 2004GL021737.

Hooper, A., Segall, P., Zebker, H., 2007. Persistent scatterer interferometric synthetic aperture radar for crustal deformation analysis, with application to Volcan Alcedo, Galapagos. J. Geophys. Res. 112, B07407. http://dx.doi.org/10.1029/ 2006JB004763.

Hou, C.S., Hu, J.C., Ching, K.E., Chen, Y.G., Chen, C.L., Cheng, L.W., Tang, C.L., Huang, S.H., Lo, C.H., 2009. The crustal deformation of the Ilan Plain acted as a westernmost extension of the Okinawa Trough. Tectonophysics 466, 344–355.

Hsieh, C.S., Shih, T.Y., Hu, J.C., Tung, H., Huang, M.H., Angelier, J., 2011. Using differential SAR interferometry to map land subsidence. a case study in the Pingtung Plain of SW Taiwan. Nat. Hazards. http://dx.doi.org/10.1007/11069- 011-9734-7.

Hsu, M.Y., 2006. Interseismic Crustal Deformation in Northern Taiwan: 1995–2005 GPS Observations. National Cheng Kung University, M.A. Thesis, 114pp.

Hu, J.C., Angelier, J., Lee, J.C., Chu, H.T., Byrne, D., 1996. Kinematics of convergence, deformation and stress distribution in the Taiwan collision area: 2-D finite-element numerical modelling. Tectonophysics 255, 243–268.

Huang, H.H., Shyu, J.B.H., Wu, Y.M., Chang, C.H., Chen, Y.G., 2012. Seismotectonics of northeastern Taiwan: structural characteristics of a transitional area from wanning collision to subduction and post-collisional extension. J. Geophys. Res. 117, B01313. http://dx.doi.org/10.1029/2011JB008852.

Jhiang, S.C., 1976. Seismic study of the Ilan Plain. Min. Tech. Dig. 14, 215–221 (in Chinese).

Kang, C.C., Emmy, T.Y., Chang Lee, J.C., Chen, R.F., 2008. Active tectonics in the Ilan Plain: geological and seismological characteristics in the conjunction between the westernmost part of the Okinawa Trough and the northernmost part of the Lishan Fault. Western Pacific Earth Sci. 8, 17–42.

Lai, K.Y., Chen, Y.G., Wu, Y.M., Avouac, J.P., Kuo, Y.T., Wang, Y., Chang, C.H., Lin, K.C., 2009. The 2005 Ilan earthquake doublet and seismic crisis in northeastern Taiwan: evidence for dyke intrusion associated with on-land propagation of the Okinawa Trough. Geophys. J. Int. 179, 678–686.

Lallemand, S., Theunissen, T., Schnürle, P., Lee, C.S., Liu, C.S., Font, Y., 2013. Indentation of the Philippine Sea plate by the Eurasia plate in Taiwan: Details from recent marine seismological experiments. Tectonophysics 594, 60–79.

Lee, C.T., Wang, Y., 1988. Quaternary stress changes in northern Taiwan and their tectonic implication. Proc. Geol. Soc. China 31, 154–168 (in Chinese).

Liang, W.T., Lee, J.C., Kuo, B.Y., 2005. Left-lateral strike-slip faulting in Ilan: Lateral extrusion at the transition between Taiwan mountain range and Okinawa Through. In: Geodynamics and Environment in East Asia International Conference & 5th Taiwan-France Earth Science Symposium, pp. 100–103.

Liu, C.C., 1995. The Ilan Plain and the Southwestward Extending Okinawa Trough. J. Geol. Soc. China 38, 183–193 (in Chinese).

Liu, C., Liu, J.P., Milliman, J.D., Lin, S., 2006. Tectonic-climatic controls on Lanyang River (Taiwan) discharge to the Southwestern Okinawa Trough. In: Ocean Science AGU Meeting 20–24 February 2006, Honolulu, Hawaii.

Massironi, M., Zampieri, D., Bianchi, M., Schiavo, A., Franceschini, A., 2009. Use of PSInSAR™ data to infer active tectonics: Clues on the differential uplift across the Giudicarie belt (Central-Eastern Alps, Italy). Tectonphysics 476, 297–303.

Massonnet, D., Feigl, K.L., 1998. Radar interferometry and its application to changes in the earth's surface. Rev. Geophys. 36, 441–500.

Okada, Y., 1985. Surface deformation due to shear and tensile faults in a half-space. Bull. Seeism. Soc. Am. 75, 1135–1154.

Rau, R.J., Ching, K.E., Hu, J.C., Lee, J.C., 2008. Crustal deformation and block kinematics in transition from collision to subduction: global positioning system measurements in northern Taiwan, 1995–2005. J. Geophys. Res. 113. http:// dx.doi.org/10.1029/2007JB005414.

Sella, G.F., Dixon, T.H., Mao, A., 2002. REVEL: a model for recent plate velocities from space geodesy. J. Geophys. Res. 107, 2081. http://dx.doi.org/10.1029/ 2000JB000033.

Shyu, J.B.H., Siesh, K., Chen, Y.G., Liu, C.S., 2005. Neotectonic architecture of Taiwan and its implications for future large earthquakes. J. Geophys. Res. 110, 1029– 2004.

Sibuet, J.C., Deffontaines, B., Hsu, S.K., Thareau, N., Le Formal, J.P., Liu, C.S.the ACT party, 1998. Okinawa Through basin: early tectonic and magmatic evolution. J. Geophys. Res. 103, 30245–30267.

Teng, L.S., 1990. Geotectonic evolution of late Cenozoic arc-continent collision in Taiwan. Tectonophysics 183, 57–76.

Tong, L.T., Ouyang, S., Guo, T.R., Lee, C.R., Hu, K.S., Lee, C.L., Wang, C.J., 2008. Insight into the geothermal structure in Chingshui, Ilan, Taiwan. Terr. Atmos. Ocean. Sci. 19 (4), 413–424.

Tsai, Y.B., 1986. Seismotectonics of Taiwan. Tectonophysics 125, 17–37.

Water Resources Agency (2015). Ground monitoring network database. <http:// pc183.hy.ntu.edu.tw/wells-and-stations.php> (March 2015).

Wells, D.L., Coppersmith, K.J., 1994. New empirical relationships among magnitude, rupture length, rupture width, rupture area, and surface displacement. Bull. Seismol. Soc. Am. 84, 974–1002.

Yu, S.B., Chen, H.Y., Kuo, L.C., 1997. Velocity field of GPS stations in the Taiwan area. Tectonophysics 274, 41–59.

Zebker, H.A., Rosen, P.A., Goldstein, R.M., Gabriel, A., Werner, C.L., 1994. On the derivation of coseismic displacement fields using differential radar interferometry: the Landers earthquake. J. Geophys. Res. 99, 19617–19634.